applied mechanics

MDPI

Article

A Newly Developed Compressed Air Cannon Test Bench Designed for Multi-Impact Analysis of Composite Structures

Ayoub Soufri [1,*], Ameur Chettah [1], Benoît Piezel [1] and Christophe Bouvet [2,*]

[1] Laboratoire DRIVE, Université de Bourgogne, 58000 Nevers, France; ameur.chettah@u-bourgogne.fr (A.C.); benoit.piezel@u-bourgogne.fr (B.P.)
[2] Institut Clément Ader, Université de Toulouse, ISAE-SUPAERO–UPS–IMT Mines Albi–INSA–CNRS, 31000 Toulouse, France
* Correspondence: ayoub.soufri@segula.fr (A.F.); christophe.bouvet@isae-supaero.fr (C.B.)

Abstract: Understanding the response and damage evolution of structures subjected to multiple impact events is essential for designing resilient structures capable of withstanding complex loading scenarios, such as impacts from hail, gravel or foreign object debris. This article presents the development and characterization of a novel test bench, the "Compressed air multi-cannon", designed specifically for studying the multi-impact behavior of composite materials. This test bench offers advantages over traditional impact testing methods by enabling controlled and adjustable impact parameters, including number of impacts, spatial and temporal lag, energy, angle and impactor dimensions. The primary objective of this work is to provide a detailed description of the test bench design, construction, and validation procedures. Key components such as the pressurized air system, projectile launch mechanism, target mounting arrangement, and data acquisition system are discussed. Experimental methodologies for assessing multi-impact response, specimen preparation, instrumentation, and data analysis techniques are outlined. Through a series of single-impact and multi-impact tests, distinctive damage mechanisms and energy absorption characteristics were observed in composite structures, revealing significant differences in how composites respond under single- and multi-impact conditions. It was found that the single-impact configuration remains particularly critical compared to multi-impact configurations with a high number of impacts. However, further testing is required to determine whether this result holds true under varying impact parameters, highlighting the unique value of this machine for exploring new, realistic questions in the literature.

Keywords: compressed air cannon; multi-impact; dynamic testing; instrument installation

Citation: Soufri, A.; Chettah, A.; Piezel, B.; Bouvet, C. A Newly Developed Compressed Air Cannon Test Bench Designed for Multi-Impact Analysis of Composite Structures. *Appl. Mech.* **2024**, *5*, 997–1010. https://doi.org/10.3390/applmech5040055

Received: 9 October 2024
Revised: 9 December 2024
Accepted: 10 December 2024
Published: 16 December 2024

1. Introduction

Composite materials are frequently exposed to impact loadings by foreign objects during manufacturing, service and maintenance operations [1]. For example, the projection of external objects such as road gravel during take-off or landing, hailstones, bird strikes or falling tools during manufacturing or maintenance operations. The induced impact damage comes in various forms such as fiber breakage, matrix cracking, fiber/matrix debonding and delamination [2]. Composite structures are particularly susceptible to the foreign impact loads because of their poor properties in the through thickness direction [3]. Consequently, the problem of impact-induced damage has attracted considerable attention in the literature ([4–6]). However, these studies generally relate to the case of an isolated impact at a single-point or repeated impacts ([7–9]). Although, in real scenarios, many structures are potentially exposed to multi-impact loading. Compared with single-point impacts, the overall structural response in multi-impact loading is modified due to a more complex damage mechanism activated by the interaction of damage induced by different projectiles [3]. The combined effects of the interaction between cracks propagation, stress

waves (especially the reflected tensile waves) and complex bending effects (leading to high local stress) is observed to govern the fracture mechanisms and the damage extent [10].

To carry out these impact tests, various types of equipment can be used ([11,12]). Typically, impact is induced using an oscillating pendulum (Izod [13] and Charpy [14]), a falling weight [15], or a projectile driven by a gas gun [16]. When the velocity and kinetic energy of a striking mass vary, energy is transferred and work is applied to the specimen (energy is absorbed through elastic and plastic deformation, hysteresis effects, friction between the specimen and test setup, and acquisition of kinetic energy by the specimen). To achieve a desired average impact velocity, the most commonly used test benches are the drop tower and gas guns [16] or Hopkinson bars [17]. For gas guns, by changing the compressing fluid, the section and length of the gun, the mass of the projectile, and the distance between the gun and the specimen, impact velocity can be varied [16].

Modern compressed air cannons for impact testing are designed with several key considerations in mind. These include optimizing the barrel length and diameter, selecting appropriate materials to withstand high pressures, and implementing sophisticated valve systems to control air release and projectile acceleration. The general configuration of a gas launcher used for high-speed impact tests consists of a pressure vessel, a firing mechanism, a launch unit, a capture chamber, and a velocity measurement unit. This type of cannon is capable of launching a projectile with an initial velocity of less than 700 m/s at a reservoir pressure of 150 bars. A higher velocity is possible if a lighter projectile and higher reservoir pressure are used ([18–20]). However, such equipment does not allow multi-impact testing, by not controlling simultaneously the key parameters that differentiate configurations (number of impacts, their location, time delay, velocity and impact energy, etc.).

To address the limitations of existing experimental setups, a newly developed compressed air cannon was designed and constructed for the multi-impact series of experiments. This advanced setup enables the study of composite structural integrity under conditions approximating real service scenarios, focusing on simultaneous or sequential multi-site impacts. This development lays the foundation for addressing critical challenges in impact dynamics, modeling, and testing. A key aspect of the compressed air cannon's design is understanding its internal dynamics, which present a complex modeling challenge. The primary question involves whether the expansion of gas accelerating the projectile follows an adiabatic or isothermal process. These distinctions are crucial for predicting the projectile's exit velocity as a function of initial gas pressure. For instance, Z. J. Rohrbach et al. [21] developed a refined model by integrating a valve mechanism into the cannon, effectively managing high-pressure gas flow while evaluating the influence of airflow dynamics. By incorporating both adiabatic and isothermal assumptions, their work improved predictions of projectile motion, enabling a deeper exploration of air drag and fundamental Newtonian kinematics. Building on this, Woojin Sung et al. [22] introduced an additional complexity—a compression wave forming ahead of the projectile during its motion through the tube. This dynamic significantly influences tube pressure and, consequently, the projectile's velocity. Their model highlights how real-world factors such as varying tube pressure result in lower maximum velocities compared to predictions assuming constant pressure. This discrepancy grows with projectile speed, illustrating the need for realistic depictions of deceleration in high-speed impact modeling.

From an experimental perspective, the unique dynamics of compressed air cannons have revealed new insights into impact damage. For example, Hosur et al. [23] demonstrated that gas cannon impacts cause more severe damage than equivalent falling-mass impacts. However, beyond a certain energy level (30 J), the laminate response becomes localized at the impact point, with similar damage patterns observed for both types of impacts. Accurate measurement of projectile velocity is a crucial aspect of compressed air cannon experimentation. Techniques such as the use of high-speed cameras, as described by P. Deconinck [24], and precision ballistic chronographs [25,26], offer reliable velocity measurements under controlled conditions. Deconinck's setup, involving parallel mirrors and laser beams, enables precise tracking of the projectile's trajectory. However, care must

be taken to align instruments with the projectile's motion while maintaining device integrity. Further innovations in measurement include Trellu et al.'s [27] use of speckle patterns on projectiles, enabling detailed motion tracking through image correlation techniques. These measurements allow the generation of impact force curves for varying shooting velocities. Similarly, advanced 3D digital image correlation (3D-DIC) systems have been employed by Wan et al. [28] to analyze mechanical responses and failure mechanisms in composite panels, providing valuable insights into structural performance under low-velocity impacts.

Despite these advancements, a significant gap remains in equipment capable of handling diverse multi-impact configurations with precise control over individual projectile parameters. While Molina-Viedma et al. [29] explored multi-impact scenarios using a single cannon, their setup lacked the flexibility to independently control projectile trajectories and velocities. In contrast, Cuadrado et al. [30] focused on sequential impacts at varying positions but were similarly limited in their ability to simulate simultaneous multi-impact conditions. The introduction of the compressed air multi-cannon by Soufri [31] addresses this gap by enabling controlled and realistic multi-impact scenarios. This innovative test bench allows for adjustable parameters such as impact energy and spatial lag, making it possible to simulate complex impact sequences encountered in real-world environments, such as hail, debris, or gravel. By bridging the limitations of previous testing setups, this new approach provides a more comprehensive understanding of composite material behavior under varied impact configurations, contributing valuable advancements to impact dynamics research.

2. Materials and Methods

2.1. Materials

Composite laminates were processed using draping method and press molding of 380 × 380 mm² unidirectional carbon fiber/epoxy prepreg, fabricated by Gurit [32], with 37% resin content and a ply thickness of 0.175 mm. The 8 plies' stacking sequence is $[0/-45/90/45]_s$, which leads to a quasi-isotropic laminate. Table 1 below summarizes the mechanical properties of the material used.

Table 1. Unidirectional material properties [32].

Property	Value (MPa)	Property	Value (GPa)
0° Tensile Strength (X_t)	2458	0° Tensile Modulus (E_t)	134
0° Compressive Strength (X_c)	1354	0° Compressive Modulus (E_{c11})	121
90° Tensile Strength (Y_T)	39.2	90° Tensile Modulus (E_{T22})	8.3
0° Flexural Strength (X_F)	1448	0° Flexural Modulus (E_{F11})	106
0° ILSS (X_{ILSS})	86.6	Fiber Modulus (E_f)	257

After curing, each specimen of dimensions 350 × 350 × 1.4 mm^3 is cut from the 380 × 380 mm² plate with a diamond bore and then measured to verify their thickness. The plates are checked by ultrasonic control (C-scan) in immersion after manufacturing to avoid possible manufacturing defects. A 25 MHz transducer (NDT Automation IU25X1-1.5) (MISTRAS GROUP SAS, Sucy-en-Brie, France) and the UltraPAC Immersion Systems device (MISTRAS GROUP SAS, Sucy-en-Brie, France) were utilized. Steel balls, 20 mm in diameter, were used as projectiles.

2.2. Methods

In the following Section of this article, the theoretical foundations for calculating cannon exit velocity are revisited, and the dimensioning parameters for the compressed air cannon are deduced based on the desired impact energy range.

2.2.1. Essential Parameters for Cannon Design

The kinetic energy at the instant of impact, E_{c_i}, of a projectile (steel ball) with mass m_p, launched from a cannon with initial air pressure P_0 towards a target plate at a distance

d from the cannon's exit, is of particular interest. The cannon is modeled as a reservoir with volume V_0, connected to a long guiding tube of length L and cross-sectional area S. The projectile is released using an electromagnetic pin, as illustrated in Figure 1.

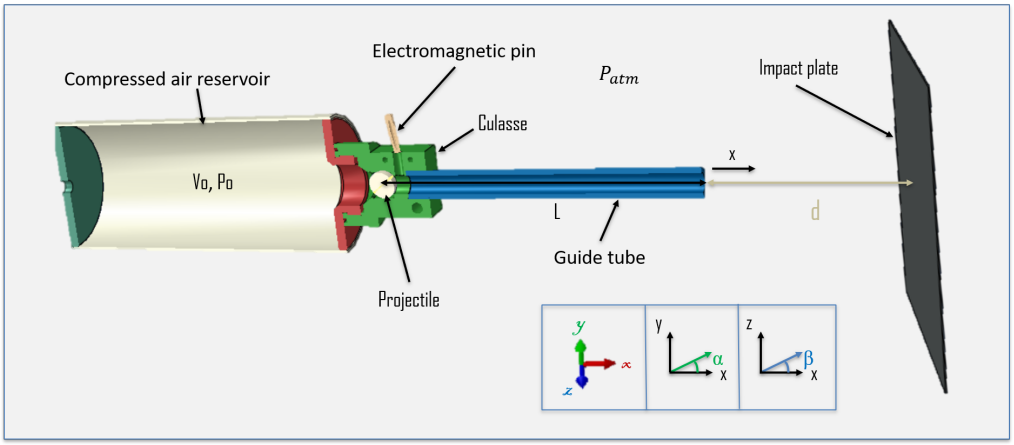

Figure 1. Cross-section of an air cannon, showing the main components (reservoir, electromagnetic pin, projectile, guiding tube), critical parameters (L, d), and angle definitions.

Once the projectile is launched along the x-axis, the volume of the cannon's reservoir $V(x)$ increases with respect to x, and the pressurized air within the reservoir, $P(x)$, expands according to Boyle–Mariotte's law:

$$P(x) = \frac{P_0 V_0}{V(x)} = \frac{P_0 V_0}{V_0 + S \cdot x} \tag{1}$$

where V_0 is the initial volume and P_0 the initial air pressure.

Assuming the projectile behaves as a rigid body, the external forces acting on it include the compressed air force $S \cdot P(x)$, the atmospheric air force $S \cdot P_{\text{atm}}$, and the frictional force F_f between the projectile and the guiding tubes, where P_{atm} is atmospheric pressure. If the cannon is positioned horizontally, the equation of motion at the cannon's exit, where the exit velocity is v_e, is given by

$$v_e = \sqrt{\frac{2}{m_p}\left(P_0 \cdot V_0 \cdot \ln\left(1 + \frac{S \cdot L}{V_0}\right) - S \cdot L \cdot P_{\text{atm}} - L \cdot F_f\right)} \tag{2}$$

Equation (2) is used to verify the cannon's repeatability (see Figure 3). Known parameters include P_{atm} and F_f, with friction accounted for by measuring it precisely using an inclined plane. The maximum air pressure P_0 is defined by the compressor's capacity (9 bars), as well as other parameters, such as m_p and S, are specified based on the scientific requirements of the tests. For steel balls with diameters of 20 mm and 10 mm, m_p is 32.7 g and 4 g, respectively.

To calculate the kinetic energy E_{c_i} at impact, it is necessary to complete the velocity calculation at the cannon exit, where the coefficient of friction is required. The maximum friction coefficient f was measured as 0.19 ± 0.02 using an inclined plane test bench. Impacts up to 50 J were chosen in order to cover a range of energies from low to medium.

As illustrated in Figure 2a, beyond a certain volume V_0 (around 0.0055 m^3), the impact energy becomes less sensitive to V_0, allowing the selection of a safe value for the final design. For example, at 4 bars, the exit velocity of the cannon varies only slightly with V_0, confirming the chosen design parameter for safety considerations.

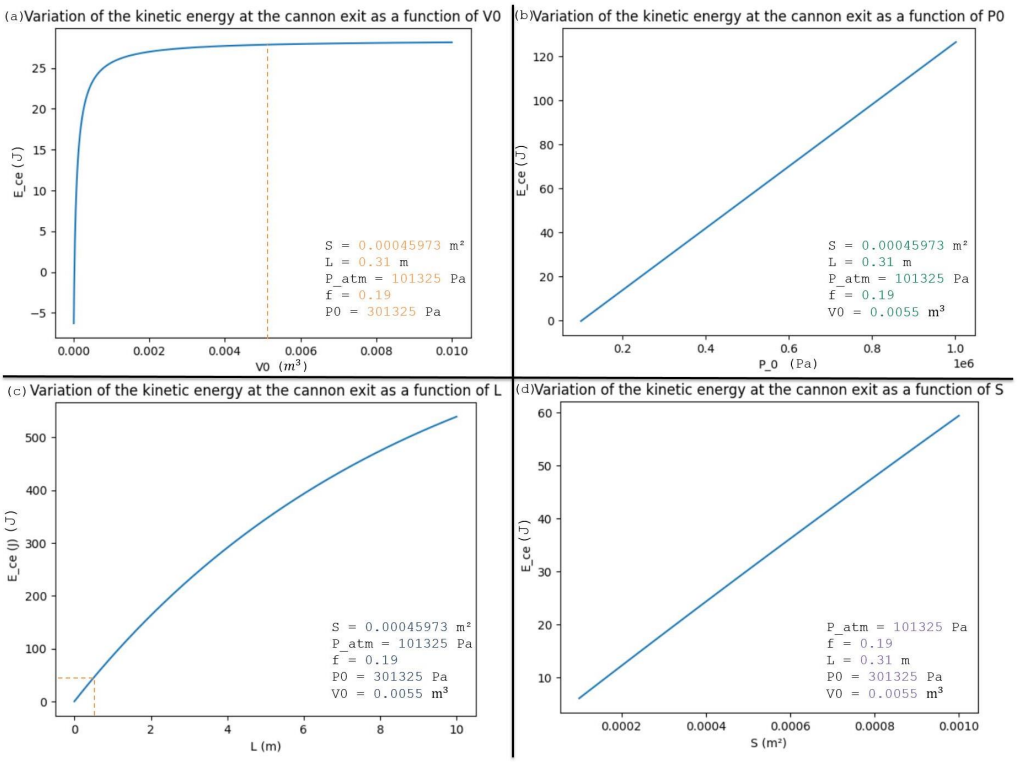

Figure 2. Kinetic energy values at the cannon's exit as a function of various design parameters (selected values shown with dotted lines).

Equation (3) is applied for sizing the cannon lengths, where $\overline{P}$ is the average pressure throughout the cannon:

$$L = \frac{v_e^2 \cdot m_p}{2 \cdot S \cdot \overline{P}} \tag{3}$$

In many experiments, the cannon is inclined to vary the impact distance or to study the effect of impact angle. The kinetic energy at impact E_{c_i}, for a ball leaving the cannon at speed v_e and at an angle α relative to the horizontal, is given by

$$E_{c_i} = \frac{m_p}{2}\left[v_e^2 - 2g \cdot d \cdot \tan(\alpha) + \left(\frac{g \cdot d}{v_e \cdot \cos(\alpha)}\right)^2\right] \tag{4}$$

This equation accounts for the influence of gravitational acceleration g on the trajectory, where d is the distance traveled from the cannon exit.

To strike the same point with two distinct impact energies, and thus with two different exit velocities from the cannon (v_1 and v_2), where v_1 represents the minimum velocity associated with the lowest energy in the experimental range, and v_2 represents the maximum velocity; the maximum allowable distance between the cannon exit and the plate d_{max} is determined using Equation (5). This distance also provides access to the area between the cannon exit and the target plate, enabling the placement of measuring instruments or other devices. A distance of 0.96 m is set, allowing impacts at 15 J and 30 J with a positional accuracy a of ± 0.50 mm within the impact zone.

$$d_{max} = \sqrt{\frac{(v_1 \cdot v_2)^2}{v_2^2 - v_1^2} \cdot \frac{2 \cdot a \cdot \cos^2(\alpha)}{g}} \tag{5}$$

To verify the repeatability of impact parameters, an experimental campaign was conducted, varying velocity, impact angle, and distance d. Exit velocities were measured

across five cannons, with a maximum error under 0.9%, validating the theoretical model with a maximum discrepancy of 6% (Figures 3 and 4).

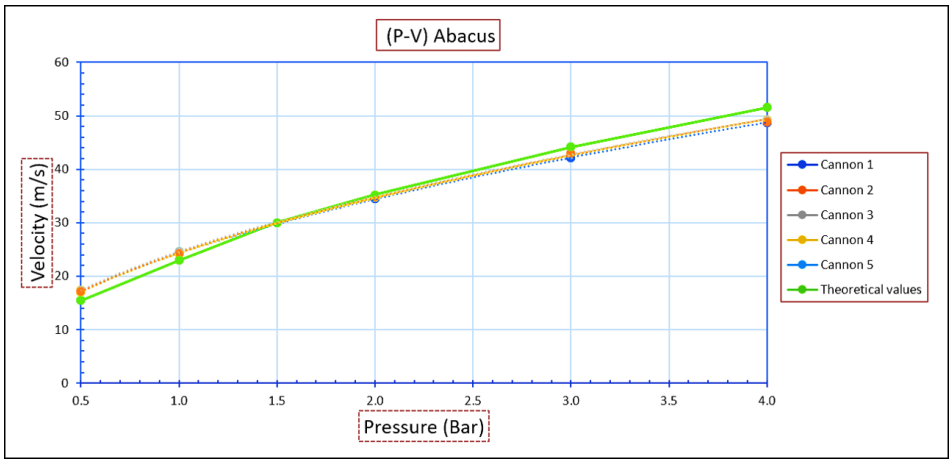

Figure 3. Experimental validation of impact velocity as a function of reservoir pressure, with comparison to theoretical calculations.

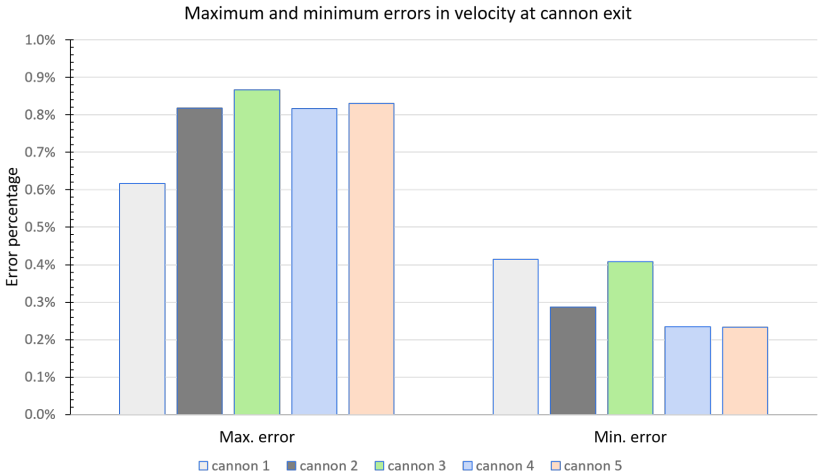

Figure 4. Maximum and minimum velocity errors at the cannon exit.

Finally, a high-speed camera was used to measure projectile velocities pre- and post-impact, providing data on kinetic energy dissipation:

$$\Delta E_c = \frac{1}{2} \cdot m_p \cdot (v_i^2 - v_f^2) \tag{6}$$

where v_i and v_f are velocities before and after impact, respectively. These data enhance our understanding of energy transfer and confirm the robustness of the cannon design for consistent and precise impact simulations.

2.2.2. Compressed Air Cannon Reservoirs

Formulas for cylindrical shells under internal pressure were referenced from the ASME code (Section VIII, Division 1, 2017), considering circumferential stress (see Figure 5a). Corrosion allowances, as required in UG-25, were incorporated, with allowable stresses referenced in Section II, Part D. Anti-corrosion protection was applied to the design, providing thickness allowances of $C_1 = 0.7$ mm and $C_2 = 0.85$ mm. For the longitudinal joints (Category A), the weld efficiency factor E was defined according to paragraph UW-12, with values ranging from 0.7 to 0.85. A safety factor of 1.5 was applied, resulting in a maximum operating pressure, P_{max}, of 13.5 bars.

The reservoir's outer diameter was set at $D_0 = 150$ mm to facilitate assembly and minimize bulk, yielding an internal diameter of $D = 145$ mm. Shell thickness was calculated to be $t_f = 2.5$ mm, with a minimum thickness requirement of $t_{min} = 0.96$ mm.

For the unstayed flat heads and covers (refer to Figure 5b), C is a factor determined by the head attachment method, shell dimensions, and other parameters as specified in the ASME Code Section VIII-Division 1- UG-34 (d); for this design, C equals 0.33. Accordingly, t_f was calculated as 10 mm, with a minimum thickness requirement of $t_{min} = 8.43$ mm.

A hydraulic test was conducted to validate the reservoirs' performance (illustrated in Figure 5c). According to the European Directive 2014/68/EU (concerning the harmonization of laws on pressure equipment), the design falls outside the scope of Article 4 of the directive. Specifically, the selected reservoir volume is 5.5 L, with a pressure limit of 9 bars. Given these values, $P.S.V = 49.5$ bar.L, which remains below the threshold of 50 bar.L for air (group II gas).

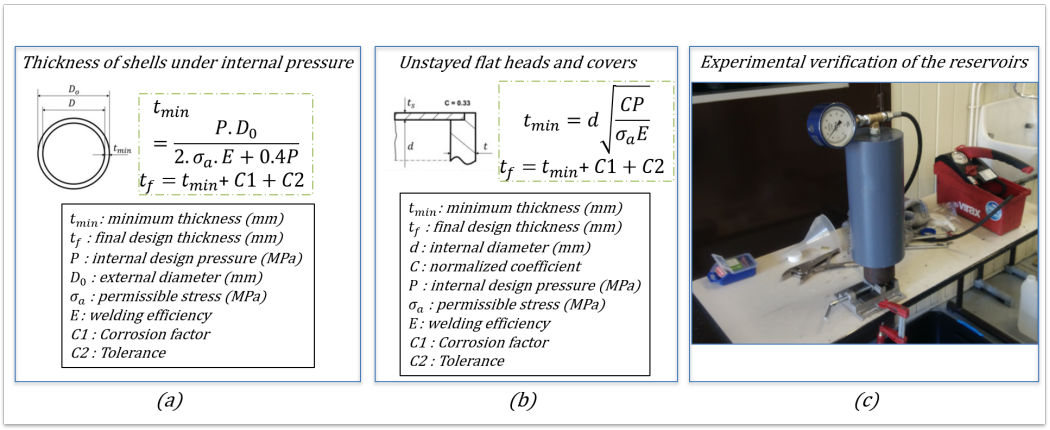

Figure 5. Design of the compressed air reservoir: (**a**) cylindrical section; (**b**) flat end cap; (**c**) hydraulic test setup.

2.2.3. Automation of Multi-Impact Testing and Data Acquisition

NI (National Instruments, Austin, TX, USA) cards were employed to facilitate real-time signal generation and data acquisition, achieving high-precision control and accurate measurement. Displacement data were acquired at 392 kHz using the NI 9222 module (National Instruments, Austin, TX, USA), which provides high-speed differential inputs with noise rejection capabilities, particularly suited for environments such as air cannons. Pressure data acquisition was performed with the NI 9205, which supports 16 channels at a 16-bit resolution with a sampling rate of 250 kS/s.

Electromagnet control was managed by the NI 9485 output module, an 8-channel device capable of handling up to 60 VDC and 750 mA per channel. This module also triggered the infrared high-speed camera with a 3.3 V TTL pulse. Data were transmitted over the network using an NI cDAQ-9189 Ethernet-enabled CompactDAQ chassis (National Instruments, Austin, TX, USA), allowing for remote control operations.

Measurement and control applications were developed in LabVIEW (2024 Q3) using these NI cards. The LabVIEW graphical interface, depicted in Figure 6a, allowed for the configuration of customized test setups and efficient data handling across multiple cannons.

To enable sequential impacts, a program was designed to initialize pressure settings for each reservoir and to select the active cannon (1 to 5). Displacement sensors were reset to zero, as shown on the LabVIEW front panel (see Figure 6b).

Signal generation across channels was controlled using NI-DAQmx and the DAQ Assistant, with a single DAQ Assistant ensuring precise timing (less than 1 ms) by utilizing a 1D array of waveforms. Each element within this array corresponds to a specific task channel, as illustrated in Figure 6b.

Figure 6. LabVIEW cannon program: (**a**) graphical interface; (**b**) front panel.

Custom scaling was applied to the instrument data using the equation $y = mx + b$, where x represents the pre-scaled voltage and y the scaled output. The parameters "m" and "b" were determined through experimental calibration or obtained from manufacturer data sheets.

3. Results

3.1. Configuration of the Test Bench

The developed air cannon system, engineered for high-precision impact testing, was installed in a dedicated test room and mounted on a robust welded structure (see Figure 7). This system includes five individually adjustable cannons that can be tilted and rotated independently to control the angle and distance of impacts.

The instrumentation setup is designed to capture high-speed data, allowing for detailed analysis of projectile impact dynamics. A FLIR X6800sc thermal high-speed camera (FLIR LLC, Wilsonville, OR, USA) records real-time thermal data during impact events, facilitating the assessment of damage in composite plates. Projectile exit speeds from the guide tubes are measured using Acetech Airsoft Gun AC6000 BT chronographs (Acetk Corp Ltd., New Taipei, Taiwan) . A MotionBLITZ EoSens® mini2 high-speed camera (Photon Lines Ltd., Banbury OX16 3ED, UK) captures projectile velocities before impact (v_i), during impact, and after impact (v_f) to provide comprehensive trajectory and speed data. Four Keyence LK-H082 laser position sensors (Keyence, Itasca, IL, USA), operating at up to 392 kHz, monitor the displacement of the target plate during impact events. Air pressure within each reservoir is monitored and controlled by Schneider Electric XMLP010BC71F pressure sensors (Schneider Electric, Minato City, Tokyo).

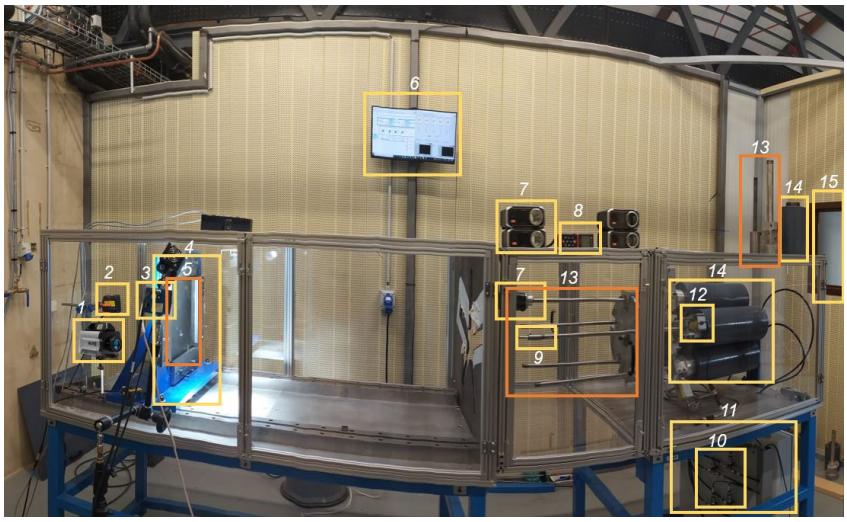

Figure 7. Compressed air cannon test bench: (1) infrared camera, (2) displacement sensors, (3) high-speed camera, (4) clamping system, (5) composite panel, (6) setup TV, (7) chronographs, (8) laser rangefinder, (9) laser sight, (10) pressure sensors, (11) electrical enclosure, (12) triggering system, (13) guiding tubes, (14) compressed air reservoirs, and (15) control room window.

3.2. Energy Verification

To verify the consistency between experimental and numerical results, it is necessary to compare the energies and forces involved during the impacts. Since force sensors cannot be fitted to the balls (due to the risk of damage), an alternative method for plotting the load–displacement curves was required. This was achieved by processing the films from the high-speed camera (HSC).

Using the HSC, the displacement of the ball was tracked to deduce the time–displacement curve (Figure 8). A polynomial function of the 6th order, which provides a more precise and realistic description of the projectile's motion under the combined influence of various forces, was fitted to the experimentally recorded points. This function strikes a balance between accuracy and model complexity.

From the equation of this curve, time–acceleration curves were plotted by calculating the second derivative of the function. This value was then multiplied by the ball's mass to calculate the force, resulting in the distance–force curve, as shown in Figure 9.

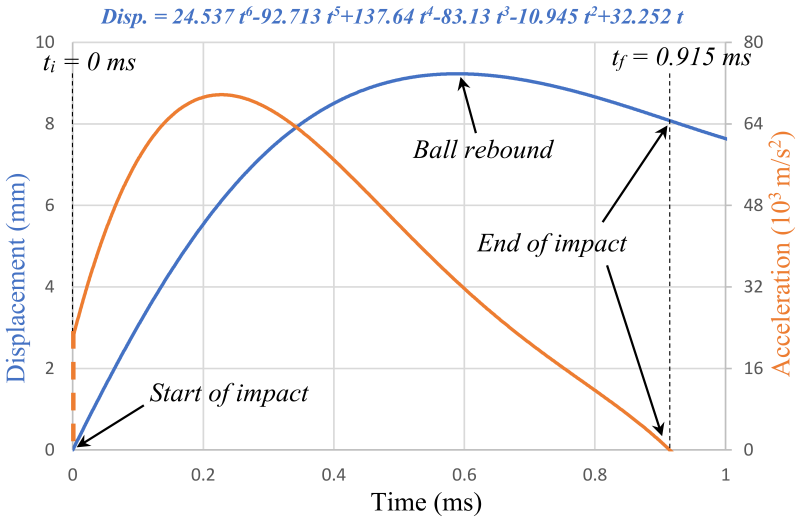

Figure 8. Displacement and acceleration curves obtained by tracking the ball's displacement with a high-speed camera.

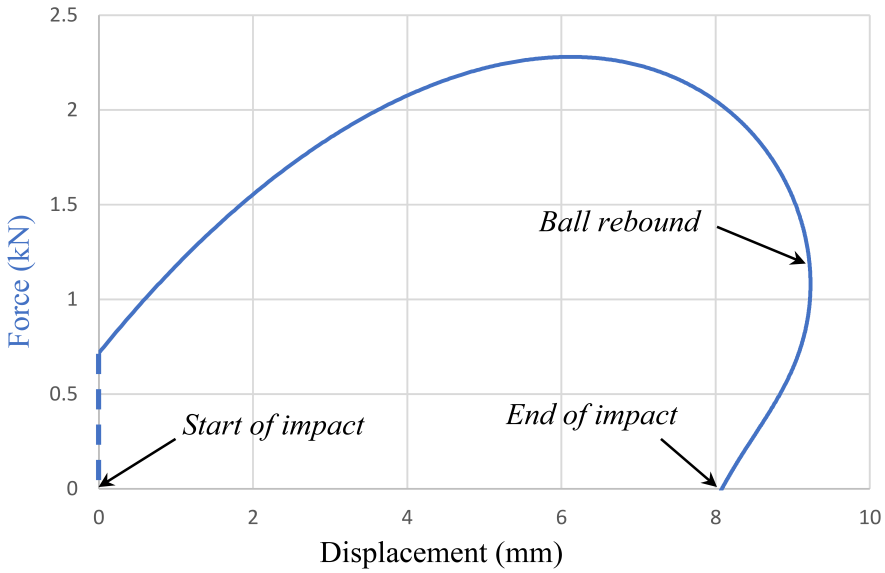

Figure 9. Force–displacement curve obtained by tracking the ball's displacement with a high-speed camera.

3.3. 30 J Mono-Impact Configuration

The 30 J mono-impact configuration involved the launch of 20 mm diameter steel projectiles at a velocity of 43 m/s. The C-scan results of the delaminated surfaces for this configuration are shown in Figure 10. Delaminations at interface 1 extended to the plate's edges, indicating the severe extent of damage. All results were based on three specimens per configuration to confirm the repeatability of the tests.

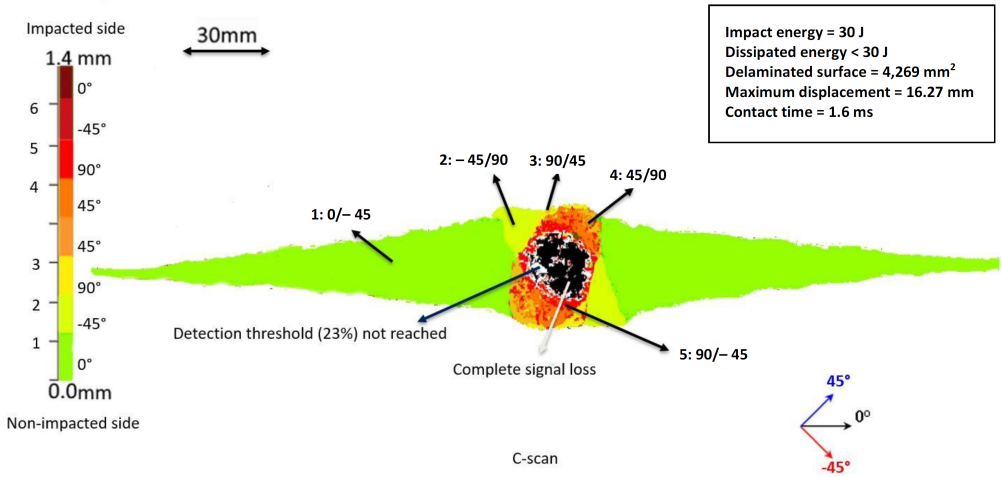

Figure 10. C-scan of 30 J mono-impact.

3.4. 6J/Ball Multi-Impact Configuration

For the multi-impact configuration, five 20 mm diameter steel projectiles were launched simultaneously at a velocity of 19 m/s, each with an energy of 6 J, totaling 30 J. The C-scan results for this configuration are presented in Figure 11, showing the delamination interfaces and their orientations within the composite material. All results were based on three specimens per configuration to confirm the repeatability of the tests.

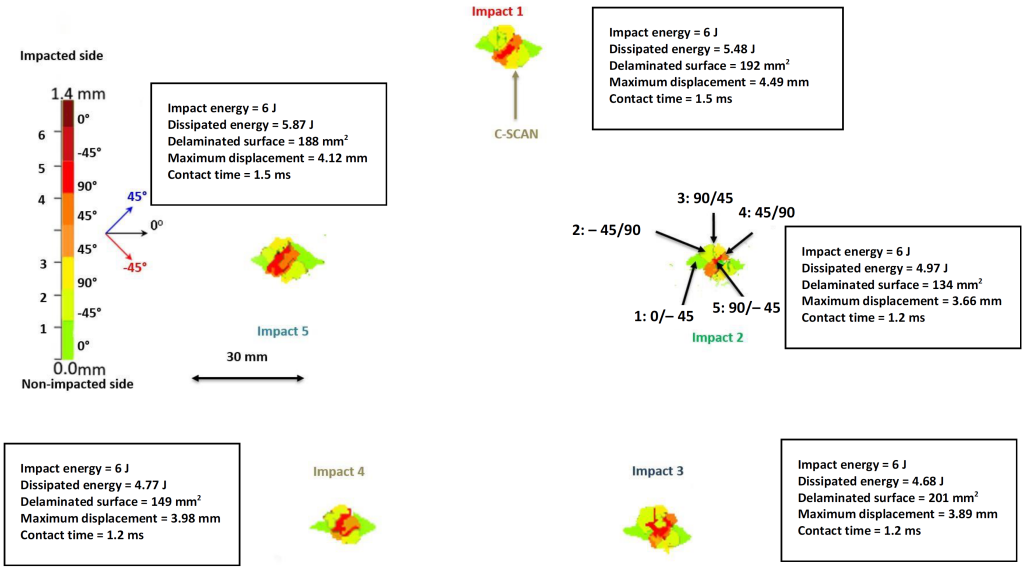

Figure 11. C-scan of 5 simultaneous impacts at a total energy of 30 J: experimental vs. numerical simulation.

4. Discussion

The results of a 30 J mono-impact configuration are discussed. This configuration is then compared to five simultaneous impacts with a maximum time lag between the first and the last impact of 1 ms, enabling a comparative analysis between a 30 J single impact and five simultaneous impacts of 6 J/ball (i.e., a total of 30 J).

The results of Figure 10 highlight the delaminated areas and their orientations, revealing extensive delamination, with the largest surface area measured at 4269 mm², with a standard deviation of 48.54 mm². During the impact, which lasted 1.6 ms, the projectile completely perforated the composite plate. This perforation rendered it impossible to accurately measure the dissipated energy, which was certainly less than 30 J since no rebound occurred. The maximum displacement (16.27 mm) and impact duration were determined from the image of the last contact between the projectile and the plate, just before complete perforation. The largest delaminated surface, situated between the 0° and −45° plies, was observed on the non-impacted side of the plate. It was oriented in the direction of the 0° plies below, with other delaminated surfaces following the orientations of the respective lower plies. At the plate's center, a black zone was visible, indicating ultrasonic signal loss caused by the projectile perforation. The signal loss was linked to the chosen synchronization threshold for the C-scan.

In contrast, the simultaneous 6 J/ball impacts, presented in Figure 11, produced significantly less damage (864 mm²) despite the total energy matching that of the single impact (30 J). The total delaminated surface area in the multi-impact case was 4.94 times smaller than in the single-impact configuration, and the delaminated surface area induced by each ball in the multi-impact case was over 21 times smaller than that in the single-impact configuration, for a comparable impact time. This finding suggests that single impacts are considerably more critical in terms of structural damage. It remains to be seen whether this conclusion is still valid for higher energies per ball and in other multi-impact configurations and for equivalent configurations (such as two nearby impacts at 15 J + 15 J).

One of the main objectives of this study was the development of the multi-impact cannon, designed to enable controlled and realistic simulations of complex impact scenarios. The successful testing of this innovative device demonstrated its capability to generate precise multi-impact configurations. This test bench allows for further exploration of complex impact scenarios, including simultaneous and sequential impacts with varying parameters such as inter-impact distance, number of impacts, and impactor size. The cannon's

capabilities open avenues for investigating cases involving gravels, hailstones, and other multi-impact phenomena.

Future studies should validate whether the observed reduction in the delaminated surface area for multi-impacts holds true for other configurations, such as 2, 3, or 4 simultaneous impacts, or for different inter-impact distances and energy levels. By leveraging the flexibility of the developed cannon, a comprehensive understanding of impact dynamics in composite materials can be achieved, advancing both research and practical applications.

5. Conclusions

The development of the compressed air multi-cannon test bench represents a significant advancement in the study of multi-impact behavior of composite structures. The test bench enables controlled simulations of various impact scenarios, with adjustable parameters such as the number of impacts, spatial and temporal lag, energy, angle, and impactor dimensions. This flexibility provides a more accurate representation of real-world multi-impact events compared to traditional testing methods. The experimental results obtained from mono-impact and multi-impact configurations highlight the importance of impact configurations in determining the extent of damage in composite materials. The findings suggest that single impacts are more damaging than multiple impacts with the same total energy. This observation has implications for the design of composite materials in applications where multi-impact events, such as hail, gravel or foreign object debris, are relevant. The test bench's capacity to simulate a wide range of impact conditions allows for a deeper understanding of the behavior of composites under complex loading. The results demonstrate that the test bench can simulate controlled multi-impact scenarios, which can be used to optimize the design of composite materials for improved performance under impact events. For example, in aerospace applications, the bench can help evaluate the response of composite structures to foreign object debris (FOD) or bird strikes, while in automotive engineering, it can aid in improving vehicle components exposed to impacts from gravel or hailstones.

Future work should focus on expanding the experimental database to include a wider range of materials and impact configurations, such as varying energy levels, inter-impact distances, and types of composite laminates. Additionally, efforts should be made to correlate experimental results with numerical models to improve the accuracy of predictive tools for multi-impact behavior. By extending these studies, a more comprehensive understanding of the performance of composite materials under multi-impact conditions can be achieved, supporting the development of more durable and reliable structures across various industries. The compressed air multi-cannon test bench provides valuable insights into the behavior of composite materials under multi-impact loading. The results contribute to the understanding of material performance and will help inform the design of more resilient structures for applications where composite materials are exposed to complex impact scenarios.

Author Contributions: Conceptualization, A.S., A.C. and B.P.; methodology, A.S., A.C., B.P. and C.B.; software, A.S. and C.B.; validation, A.S., A.C., B.P. and C.B.; formal analysis, A.S., A.C., B.P. and C.B.; investigation, A.S., A.C., B.P. and C.B.; data curation, A.S. and C.B.; writing—original draft preparation, A.S.; writing—review and editing, A.S. and C.B.; visualization, A.S. and C.B.; supervision, A.C., B.P. and C.B.; project administration, A.C., B.P. and C.B.; funding acquisition, A.C. and B.P. All authors have read and agreed to the published version of the manuscript.

Funding: This work was conducted at the DRIVE laboratory at ISAT in Nevers. This research was funded by the Bourgogne-Franche-Comté Region and the SPIM Doctoral School (ED37).

Institutional Review Board Statement: Not applicable.

Informed Consent Statement: Not applicable.

Data Availability Statement: The original contributions presented in this study are included in the article. Further inquiries can be directed to the corresponding authors.

Acknowledgments: We would like to thank the Clément Ader Institute (ICA, CNRS UMR 5312) for the use of the CALMIP computing facility.

Conflicts of Interest: The authors declare no conflicts of interest.

References

1. Cesari, F.; Dal Re, V.; Minak, G.; Zucchelli, A. Damage and residual strength of laminated carbon–epoxy composite circular plates loaded at the centre. *Compos. Part Appl. Sci. Manuf.* ***2007***, 38, 1163–1172. [CrossRef]
2. Xiao-Yu, S.; Jian-Xin, T.; Zheng, H.; Xuan, G. A study on the failure mechanisms of composite laminates simultaneously impacted by two projectiles. *Adv. Compos. Lett.* ***2018***, 27, 96–106. [CrossRef]
3. Abrate, S. *Impact Engineering of Composite Structures*; CISM International Centre for Mechanical Sciences; Springer: Vienna, Austria, 2011; pp. 97–128.
4. Wang, C.; Yew, C.H. Impact damage in composite laminates. *Comput. Struct.* ***1990***, 37, 967–982.
5. Davies, G.A.O.; Olsson, R. Impact on composite structures. *Aeronaut. J.* **2004**, 542 –561. [CrossRef]
6. Cantwell, W.J.; Worton, J. Comparison of the low and high velocity impact response of CFRP. *Compos. J.* ***1989***, 20, 545–551. [CrossRef]
7. Mokhtar, H.B. Contribution to the Study of Impact Damage on Composite Laminates: The Effect of Hygrothermal Ageing and Preloading. Ph.D Thesis, University of Burgundy, Nevers, France , 2012; pp. 78–85.
8. Amouzou, A.S.E.; Sicot, O.; Chettah, A.; Aivazzadeh, S. Experimental characterization of composite laminates under low-velocity multi-impact loading. *J. Compos. Mater.* **2019**, *53*, 2391–2405. [CrossRef]
9. Amaro, A.; Reis, P.; Moura, M.; Neto, M. Influence of multi-impacts on GRP composite laminates. *Compos. Part* **2013**, *52*, 93–99. [CrossRef]
10. Bartus, S. Simultaneous and Sequential Multi-Site Impact Response of Composite Laminates. Ph.D Thesis, The University of Alabama at Birmingham, Birmingham, AL, USA, 2006; p. 49.
11. Hall, Z.E.C.; Liu, J.; Brooks, R.A.; Liu, H.; Dear, J.P. Impact testing on the pristine and repaired composite materials for aerostructures. *Appl. Mech.* ***2023***, 4, 421–444. [CrossRef]
12. Safri, S.N.A.; Sultan, M.T.H.; Yidris, N.; Mustapha, F. Low velocity and high velocity impact test on composite materials—A review. *Int. J. Eng. Sci. (IJES)* **2014**, *3*, 50–60.
13. Costa, U.O.; Nascimento, L.F.C.; Garcia, J.M.; Bezerra, W.B.A.; Monteiro, S.N. Evaluation of Izod impact and bend properties of epoxy composites reinforced with mallow fibers. *J. Mater. Res. Technol.* **2020**, *9*, 373–382. [CrossRef]
14. Hufenbach, W.; Ibraim, F.M.; Langkamp, A.; Böhm, R.; Hornig, A. Charpy impact tests on composite structures—An experimental and numerical investigation. *Compos. Sci. Technol.* **2008**, *68*, 2391–2400. [CrossRef]
15. Sfarra, S.; Ibarra-Castanedo, C.; Santulli, C.; Paoletti, A.; Paoletti, D.; Sarasini, F.; Bendada, A.; Maldague, X. Falling weight impacted glass and basalt fibre woven composites inspected using non-destructive techniques. *Compos. Part Eng.* **2013**, *45*, 601–608. [CrossRef]
16. VanderKlok, A.; Stamm, A.; Dorer, J.; Eryi, H.; Auvenshine, M.; Pereira, J.M.; Xiao, X. An experimental investigation into the high velocity impact responses of S2-glass/SC15 epoxy composite panels with a gas gun. *Int. J. Impact Eng.* **2018**, *111*, 244–254. [CrossRef]
17. Gama, B.A.; Lopatnikov, S.L.; Gillespie, J.W., Jr. Hopkinson bar experimental technique: A critical review. *Appl. Mech. Rev.* **2004**, *57*, 223–250. [CrossRef]
18. Sultan, M.T.H.; Basri, S.; Rafie, A.S.M.; Mustapha, F.; Majid, D.L.; Ajir, M.R. High velocity impact damage analysis for glass epoxy laminated plates. *Adv. Mater. Res.* **2012**, *399–401*, 2318–2328. [CrossRef]
19. Lamberson, L. Investigations of high-performance fiberglass impact using a combustionless two-stage light-gas gun. *Procedia Eng.* **2015**, *103*, 341–348. [CrossRef]
20. Zhou, H.; Jing, K.; Xie, S.; Feng, Z.; Wang, H. Experiment of high-speed cumulative impact of carbon fiber plate based on air cannon. *Sci. Technol. Compos. Mater.* **2023**, *40*, 29–35.
21. Rohrbach, Z.J.; Buresh, T.R.; Madsen, M.J. Modeling the exit velocity of a compressed air cannon. *Am. J. Phys.* **2012**, 24–26 . [CrossRef]
22. Woojin, S.; Jihoon, K.; Kyeong, S.J.; Thi, T.G.L.; Jeonglae, K.; Dong, H.K.; Hyoungsoon, L.; Jaiyoung, R. Parametric study of a projectile launched by a compressed air cannon. *J. Mech. Sci. Technol.* **2023**, *37*, 5913–5933.
23. Hosur, M.V.; Murthy, C.R.L.; Ramamurthy, T.S.; Shet, A. Estimation of impact-induced damage in CFRP laminates through ultrasonic imaging. *NDT E Int.* **1998**, *31*, 359–374. [CrossRef]
24. Deconinck, P. Étude du Comportement à l'Impact de Matériaux Composites Renforcés par Tufting. Ph.D. Thesis, University of Lorraine, Nancy, France, 2014; pp. 13–16.
25. Mukhammad, A.F.H.; Nurhadiyanto, D.; Hassan, S.A.; Riyadi, T.W.B. Preliminary study of fragment simulating projectile on epoxy-ramie composite. *J. Phys. Conf. Ser.* **2020**, *1446*, 012001. [CrossRef]
26. Ari, A.; Karahan, M.; Ahrari, M. The effect of manufacturing parameters on various composite plates under ballistic impact. *Polym. Polym. Compos.* **2022**, *30*, 09673911221144874 [CrossRef]

27. Trellu, A.; Bouvet, C.; Rivallant, S.; Ratsif, R.L.; Chardonneau, A. Simulation d'Impact à Moyenne Vitesse et de Compression ou Cisaillement Après Impact sur Grandes Plaques Composites Stratifiées. JNC21 (21ème Journées Nationales sur les Composites). 2019, 1–7. Available online: https://hal.science/hal-02420721/ (accessed on 8 December 2024).
28. Wan, Y.; Liu, Y.; Hu, C.; Yao, J.; Wang, F.; Yang, B. The failure mechanism of curved composite laminates subjected to low-velocity impact. *Acta Mech. Sin.* **2023**, *39*, 2–10. [CrossRef]
29. Molina-Viedma, Á; López-Alba, E.; Felipe-Sesé, L.; Díaz, F. Full-field operational modal analysis of an aircraft composite panel from the dynamic response in multi-impact test. *Sensors* **2021**, *21*, 1602. [CrossRef] [PubMed]
30. Cuadrado, M.; Pernas-Sanchez, J.; Artero-Guerrero, J.A.; Varas, D. Detection of barely visible multi-impact damage on carbon/epoxy composite plates using frequency response function correlation analysis. *Measurement* **2022**, *196*, 111194. [CrossRef]
31. Soufri, A. Multi-Impact Behavior of Composite Structures: Experimental and Numerical Approach. Ph.D Thesis, University of Burgundy, Nevers, France, 2023; pp. 49–76.
32. Gurit. SE 84LV: Epoxy-Based Prepreg Curing at Low Temperature (SE84LV-25-0519). 2007. Available online: https://www.gurit.com/ (accessed on 8 December 2024) .